International Journal of Recent Innovations in Academic Research
E-ISSN: 2635-3040; P-ISSN: 2659-1561
Homepage: https://www.ijriar.com/
Volume-9, Issue-3, July-September-2025: 337-344

Research Article

Electrical and Electrochemical Characterisation of Sol-Gel Prepared Magnesium Hafnium Phosphate Solid Electrolyte for Magnesium-Sensors

[a,b,c,*]Mohammed Alhaji Adamu and [c]Girish M Kale

[a]Department of Metallurgical and Materials Engineering Technology, Kogi State Polytechnic, Lokoja, Nigeria
[b]Engineering Materials Research Group, Kogi State Polytechnic, Lokoja, Nigeria
[c]School of Chemical and Process Engineering, University of Leeds, Leeds LS2 9JT, United Kingdom
*Corresponding Author Email: drmadamu@yahoo.com

Received: August 23, 2025 **Accepted:** September 14, 2025 **Published:** September 20, 2025

Abstract
Magnesium hafnium phosphate, $MgHf_4P_6O_{24}$ solid electrolyte with an alkali 8.9 pH was produced using the sol-gel process. Electrical and electrochemical characterisation of the solid electrolyte were determined. TGA-DSC analysis indicated that the dried xerogel powder, when calcined at 900 ^oC for 3 h converts to single phase $MgHf_4P_6O_{24}$ solid electrolyte nanopowders. Pellets of 13 mm diameter and 3.8 mm thickness made by uniaxial compression were sintered at 1300 ^oC for 24 h. The platinium-cured pellets exhibited ionic conductivity of 4.52 x 10^{-4} Scm^{-1} and activation energy of 0.74 ± 0.02 eV at 747 ^oC. The electrical and electrochemical properties of this sol-gel prepared solid electrolyte together with the reference electrode, $MgCr_2O_4+Cr_2O_3+O_2$ biphasic powder mixture, finds suitable applications in Mg-sensors and other electrochemical devices.
Keywords: Solid Electrolyte, $MgHf_4P_6O_{24}$, Reference Electrode, Mg-Sensor, Electrochemical Devices.

1. Introduction

Sol-gel process provides a unique approach to the preparation of ceramic materials (Livage *et al.,* 1988) where the homogeneous materials can be easily obtained by mixing the molecular precursor solution (Dislich, 1971; Zelinski and Uhlmann, 1984). The sol-gel process is an attractive alternative to other methods available for the synthesis of ceramic materials (Brinker *et al.,* 1991; Hu *et al.,* 1992; Brinker and Scherer, 2013). The sol-gel process is gaining rapid popularity for large-scale production of fine ceramics (Pathak and Pramanik, 2001). A feature of this study, particularly for solid electrolytes, is the interdisciplinary nature and important contribution chemistry is making to the development and manufacture of solid electrolyte nanopowders (Segal, 1996; Segal, 1997). In a recent study, experimental data on the structural and thermal properties of sol-gel prepared $MgHf_4P_6O_{24}$ solid electrolyte have been published (Adamu and Kale, 2025). However, data on the electrical and electrochemical properties of the solid electrolyte and other phosphate-based solid electrolytes are scarcely reported.

Sol-gel process was adopted for use in this study due to its potential advantage of yielding ceramic materials with homogeneous phase and high-density compacts at a noticeably low temperature (Mackenzie, 1985; Adamu and Kale, 2016; Mustaffa and Mohamed, 2016; Joost and Krajewski, 2017; Judez *et al.,* 2018; Adamu *et al.,* 2020; Adamu and Kale, 2025) when compared with conventional solid-state reactions between oxide powders (Tamura *et al.,* 2004; Tamura *et al.,* 2016). Sol-gel process have shown enormous impact on the electrical behaviour of bulk $MgZr_4P_6O_{24}$ solid electrolyte (Adamu and Kale, 2016; Mustaffa and Mohamed, 2016; Adamu *et al.,* 2020) with suitable applications in Mg-sensors and other electrochemical devices, and thermodynamic analysis at high temperatures in aggressive environment (Mudenda and Kale, 2017; Sivasankaran and Kumar, 2019).

Producing the next-generation of electrochemical devices, for instance, univalent and divalent batteries, fuel cells and chemical sensors that are superior to the lithium-ion powered devices, in terms of cost, safety and energy storage capacity, has become a crucial task and at the heart is the solid electrolytes representing the

key components for creating electrochemical devices with these desirable properties (Mustaffa and Mohamed, 2016). Among the class of solid electrolytes, ceramic electrolytes form a significant class because they possess wide electrochemical stability window, absence of leakage compared to liquid electrolytes and can be fabricated into a variety of sizes and shapes (Knauth, 2009; Fergus, 2012).

In furtherance of our research interests on phosphate-based solid electrolytes, we are reporting for the first time, the electrical and electrochemical properties of $MgHf_4P_6O_{24}$ solid electrolyte and its applications in Mg-sensors, incorporating the reference electrode, $MgCr_2O_4$+Cr_2O_3+O_2 biphasic powder mixture for in-line monitoring of dissolved Mg in a primary or secondary molten non-ferrous alloys at 700±5 ^oC.

2. Experimental Method

2.1. Materials Synthesis

Analytical grade precursor $Mg(NO_3)_2$ chemical powders from Sigma-Aldrich Chemical Co Ltd (Gillingham, Dorset, UK), $HfCl_4$ and $NH_4H_2PO_4$ from Alfa Aesar Fine Chemicals and Metals (Heysham, Lancashire, UK) were used as received to produce $MgHf_4P_6O_{24}$ nanopowders, akin to the process used in an earlier study (Adamu and Kale, 2025). Appropriate stoichiometric amounts of analytical grade of the precursor materials used were weighed and dissolved in separate beakers of distilled water labelled A, B, C as presented in Figure 1. Beaker A contains $Mg(NO_3)_2$ aqueous solution, Beaker B contains $NH_4H_2PO_4$ aqueous solution while Beaker C contains $HfCl_4$ aqueous solution. To produce the sol, $Mg(NO_3)_2$ and $NH_4H_2PO_4$ aqueous solutions were mixed together while stirring in beaker D with a magnetic stirrer at room temperature. Appropriate amount of $HfCl_4$ aqueous solution was prepared separately and then added dropwise to the prepared homogeneous sol using a burette to produce white wet gel. To neutralise the mixture, concentrated NH_4OH was gradually added dropwise to the white wet gel to adjust the initial acidic 0.2 pH to a final alkali 8.9 pH. The final white wet gel was stirred for 0.5 h and dehydrated at 100 ^oC for 24 h on a hot plate to achieve dried xerogel powders. After the dehydration process, the xerogel powders were mechanically ground with an agate mortar and pestle into fine xerogel powders.

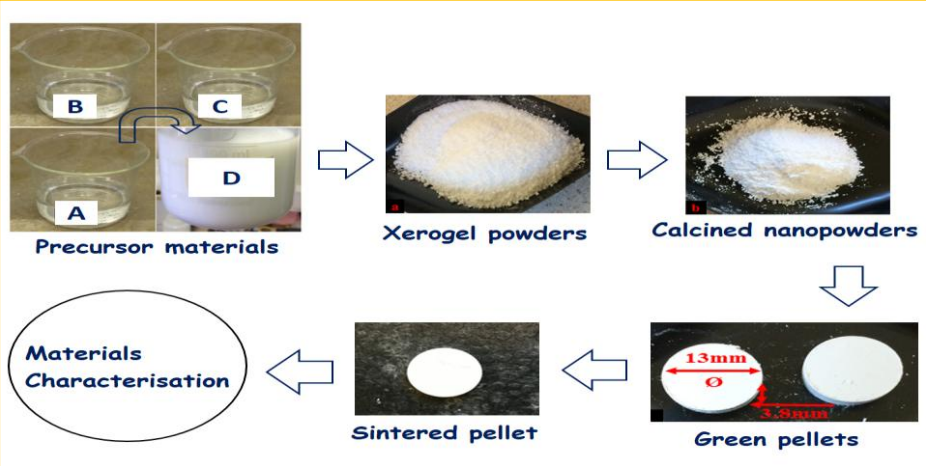

Figure 1. Sol-gel process of prepared $MgHf_4P_6O_{24}$ solid electrolyte (Adamu and Kale, 2025).

The ground fine xerogel powders was then analysed for its weight loss and heat flow as a function of temperature. After the TGA-DSC analysis, the dried xerogel powder was calcined at 900 ^oC for 3 h in a top loading muffle furnace using data from the TGA-DSC analysis. The calcined nanopowders mixed with 1 wt.% binder, Ciba Glascol HA4, was subsequently dried at 100 ^oC for 0.5 h and pressed into pellets of 13 mm diameter and 3.8 mm thickness using uniaxial compression, akin to the pellet-making procedure adopted in an earlier study (Adamu and Kale, 2025). The resultant green pellets were initially heated between 400-450 ^oC for the purpose of burning out the binder prior to sintering at 1300 ^oC for 24 h at a heating rate of 10 ^oC min^{-1}. During sintering, the pellets were embedded in a calcined nanopowder of the same composition in a closed alumina crucible in order to protect the loss of volatile oxides, like P_2O_5 at high-temperatures (Collin and Boilot, 1989). This procedure will also prevent any potential reaction between the alumina crucible and the solid electrolyte pellets by enabling the calcined nanopowders as a sacrificial material. This may also limit the loss of possible volatiles during sintering.

2.2. Materials Characterisation

The prepared xerogel powders was subjected to thermal analysis; thermogravimetric analysis and differential scanning calorimetry (TGA-DSC) using STA 8000 (PerkinElmer, Seer Green, UK) for thermal

oxidation behaviour and weight loss of the dried xerogel powders. The analysis ensured effective optimisation of calcination conditions of the xerogel powders in a controlled atmosphere at a flow rate of 50 mL min^{-1} using a constant heating-cooling rate at 10 ^oC min^{-1} between 30 to 1000 ^oC, akin to that described in our previous papers (Adamu and Kale, 2016; Adamu *et al.,* 2020; Adamu and Kale, 2025). The resultant dried xerogel powders were calcined at 900 ^oC for 3 h, and then pressed into pellets of 13 mm diameter and 3.8 mm thickness using uniaxial compression. The pressed pellets were then sintered at 1300 ^oC for 24 h at a 10 ^oC min^{-1} heating-cooling rate in a closed alumina crucible immersed in powders of the calcined sample composition. Phase analysis for both the calcined nanopowders and sintered pellets of $MgHf_4P_6O_{24}$ solid electrolyte were examined using powder x-ray diffractometer, XRD (Bruker D8 Advance, Karlsruhe, GmbH) equipped with $CuK_{\alpha 1}$ (with λ = 1.5406 Å) radiation source operating at 30 kV and 45 mA, and calibrated against Si standard, and the XRD data was collected over $10° \leqslant 2\theta \leqslant 80°$ scan range.

For electrical and electrochemical characterisation, the platinum-cured pellets for impedance analysis were prepared by lightly grinding the two flat surfaces of the pellets sequentially on dried surfaces of silicon carbide (SiC) papers with grit size P2500. Afterwards, geometric measurements on the ground pellets to determine the thickness and diameter of the solid electrolyte was achieved. Thereafter, the pellets were platinised by applying platinum paste and cured at 800 ^oC for 0.5 h to provide good adhesion between platinum paste and the solid electrolyte pellets thereby forming contact electrode. The platinium-cured pellet was spring loaded in a quartz assembly rig placed inside a Faraday cage within horizontal Lenton LTF1200 tube furnace (Lenton Thermal Designs Ltd., Market Harborough, UK). A type-K thermocouple was inserted close to the spring-loaded pellet to monitor the actual impedance temperature. Actual impedance temperatures of $25\,^oC \leqslant T \leqslant 800\,^oC$ were monitored and recorded through a plug and play temperature input device, the NI USB-TC01 connected to a LabVIEW interface (Business Park, Newbury, UK). The platinum wire clips were then connected to the Solartron SI1260 FRA impedance analyser which interfaced with a computer controlled by the software ZPlot (Scribner Associates, Inc. USA).

The electrochemical Mg-sensor characterised in this study was prepared using high conducting $MgHf_4P_6O_{24}$ solid electrolyte, a non-reactive annealed Fe-Cr alloy wire, Mo-rod counter electrode and reference electrode, $MgCr_2O_4$+Cr_2O_3+O_2 biphasic powder mixture. Dense $MgHf_4P_6O_{24}$ solid electrolyte pellets were respectively attached to open end 50.8 mm long alumina tubes using pure alumina refractory cement (Parkinson-Spencer Refractories Ltd., Halifax, UK) to form exclusive alumina probes. A 0.25 mm thick annealed Fe-Cr alloy wire (Goodfellow, Cambridge) was coiled, inserted and rammed into bottom of the alumina probes along with $MgCr_2O_4$+Cr_2O_3+O_2 biphasic powder mixture. The prepared Mg-sensors were respectively inserted into 120 mm shock resistant SiAlON ceramic tubes and held firmly with alumina refractory cement, as presented in Figure 2.

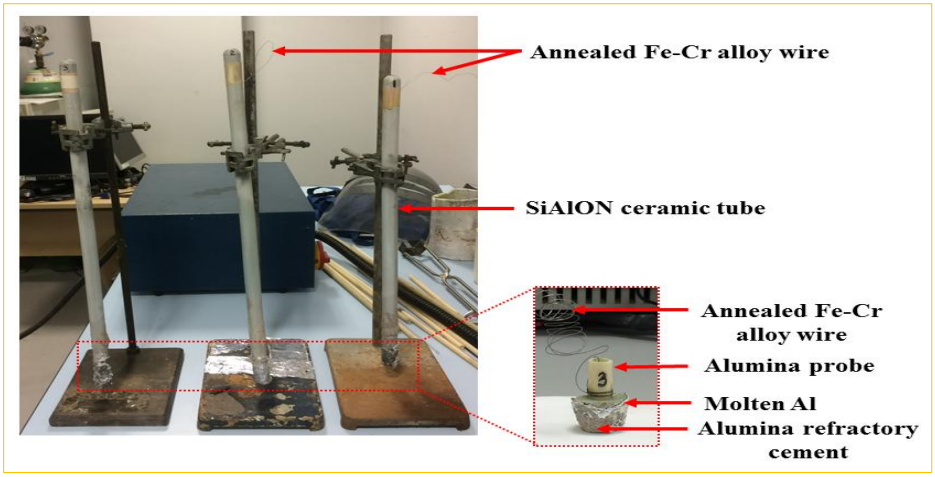

Figure 2. Bulk electrochemical Mg-sensors showing the Mg-sensor before insertion in SiAlON ceramic tube.

3. Results and Discussions

3.1. Thermal Analysis (TGA-DSC)

Phase formation and possible transformation temperatures of $MgHf_4P_6O_{24}$ solid electrolyte was determined using TGA-DSC. The main decomposition changes on the TGA profiles in Figure 3 shows that dehydration of lattice H_2O occurred within 30-100 ^oC, while from 150 ^oC to 500 ^oC, the weight loss observed may result from decomposition or oxidation of the inorganic precursors; $Mg(NO_3)_2$, $HfCl_4$ and $NH_4H_2PO_4$. Similarly, DSC profiles of the dried xerogel powders identified two endothermic decomposition peaks at 150 ^oC and 350 ^oC,

and exothermic peak at 900 °C. Decomposition of $NH_4H_2PO_4$ into $(NH_4)_3H_2P_3O_{10}$ and H_2O molecules within 140-170 °C could be responsible for the endothermic peak observed at 150 °C. Also, the decomposition of $Mg(NO_3)_2$ into MgO, NO_2 and O_2 at a temperature above 300 °C, could be responsible for the endothermic peak at 350 °C. The reactive oxide HfO_2 formed by the oxidation of $HfCl_4$ at 432 °C produced the solid electrolyte after stoichiometric reaction with MgO and P_2O_5 reactive oxides at 900 °C (Adamu *et al.,* 2020; Adamu and Kale, 2025). Therefore, the exothermic peak observed at 900 °C depicts the formation of $MgHf_4P_6O_{24}$ solid electrolyte. However, TGA profile shows the initial formation stage and stability temperature of the solid electrolyte at 780 °C.

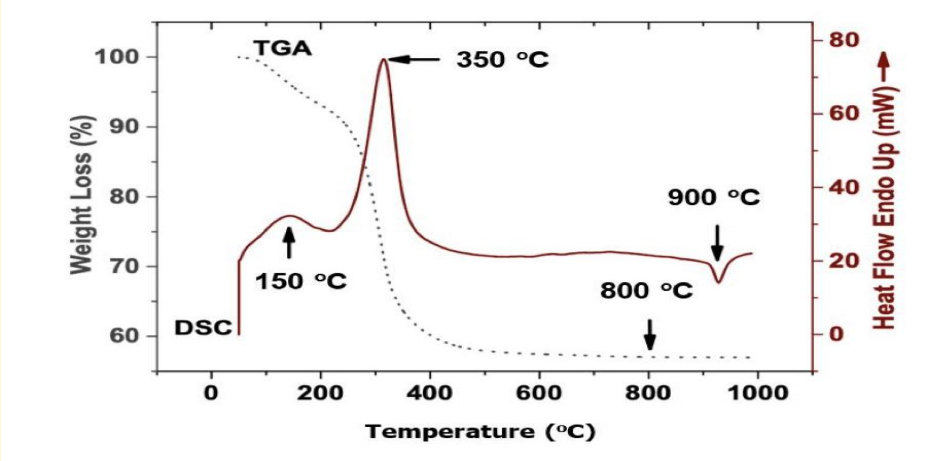

Figure 3. TGA-DSC profiles of $MgHf_4P_6O_{24}$ xerogel powders at scan rate of 10 °C min^{-1} in the air (Adamu and Kale, 2025).

3.2. X-Ray Diffraction (XRD)

The XRD patterns of $MgHf_4P_6O_{24}$ solid electrolyte nanopowders calcined at 900 °C for 3 h and the pellets sintered at 1300 °C for 24 h is presented in Figure 4 with all the peaks fully matched and indexed to ICDD-04-016-0487 and ICDD-04-011-6948.

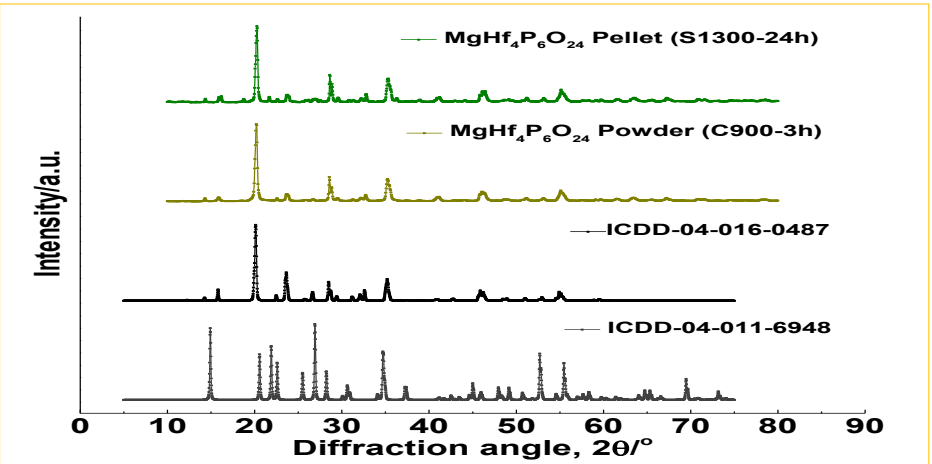

Figure 4. Combined XRD peaks of pure $MgHf_4P_6O_{24}$ nanopowders calcined at 900 °C for 3 h and pellets sintered at 1300 °C for 24 h. All peaks indexed to ICDD-04-016-0487 and ICDD-04-011-6948 (Adamu and Kale, 2025).

3.3. Electrochemical Impedance Analysis (EIA)

Electrochemical impedance analysis of the platinium-cured $MgHf_4P_6O_{24}$ solid electrolyte pellet is presented as Nyquist plots in Figure 5. The analysis demonstrates the electrical properties of Mg^{2+}-ion conducting specie in $MgHf_4P_6O_{24}$ solid electrolyte. It further identifies the contribution from the grain interior, grain boundary and electrode-electrolyte interface in the high, intermediate and low frequency regions of the Nyquist plots (Bauerle, 1969). The impedance spectra measured in this study falls within the 182–747 °C temperature and 100 mHz-32 MHz frequency range.

The impedance spectra in Figure 5(a) shows a single slightly depressed semicircle at higher-frequency followed by the low-frequency spike inclined at angle 45°. The appearance of such inclined spike at low-

frequency demonstrates $MgHf_4P_6O_{24}$ solid electrolyte as an ionic conductor (Irvine *et al.,* 1990; Huggins, 2002). The slightly depressed semicircle is attributed to the CPE parameter which suggests non-Debye type relaxation behaviour (MacDonald, 1987) since the centre of the depressed semicircle is located below the axis, this electrochemical impedance behaviour is similar to those observed in other solid electrolytes (Chowdari and Gopalakrishnan, 1986).

The slightly depressed semicircle could have resulted from ionic migration in the bulk solid electrolyte which is indicative that the solid electrolyte pellet is dense and well sintered, and it confirms the absence of grain boundary effects. Furthermore, inclined spike observed in the low-frequency region may be attributed to the polarisation effect at the electrode-electrolyte interface (Ferloni and Magistris, 1994). The border frequency, f_b in Figure 5 corresponds to 6.38 kHz, 1.60 kHz and 2.02 kHz for $MgHf_4P_6O_{24}$ solid electrolyte at 273 °C, 690 °C and 747 °C, respectively.

As impedance temperature increases from 273 °C in Figure 5(a) to 690 °C and then 747 °C in Figure 5(b), the depressed bulk semicircle gradually becomes smaller and the inclined spike on the electrode-electrolyte interface gradually bent downward to become a depressed semicircle. This implies that as the bulk resistance, R_b is decreasing, the reversibility of charge migration at electrode-electrolyte interface is increasing (Bo *et al.,* 2006). Furthermore, the semicircles seen in Figure 5(b) are not starting from the origin, implying there is a finite resistance, R_s representing a lumped electrode-electrolyte interfacial resistance in series with a parallel combination of R_b and CPE_b representing constant phase element, CPE.

Electric modulus in Figure 5(a) and Figure 5(b) illustrates relaxation dynamics of the ionic species. Variations of imaginary component (M''/C_o) as a function of frequency (ω) at different temperatures show the resolved peaks at unique peak frequencies, with the peaks displaying a tendency to shift towards a higher frequency region with increase in temperature. This behaviour suggests a thermally activated conduction mechanism with correlated hopping of Mg^{2+}-ions.

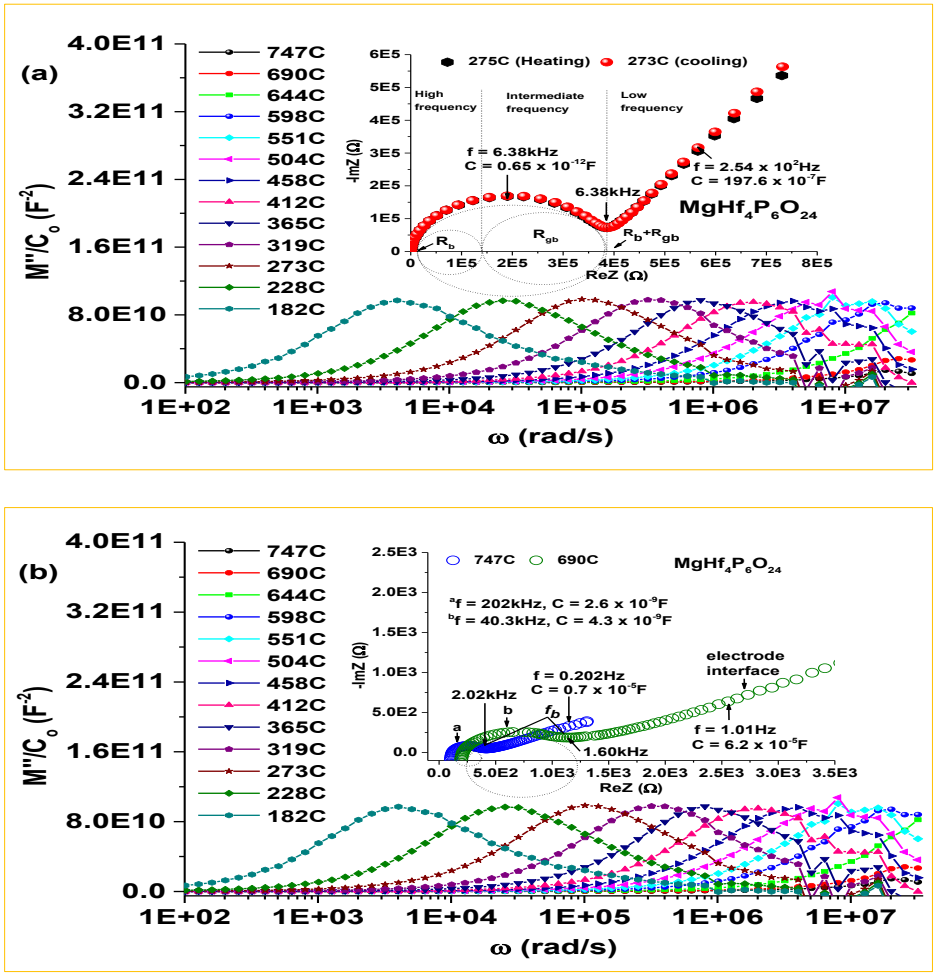

Figure 5. Nyquist plots and electric modulus of $MgHf_4P_6O_{24}$ solid electrolyte at (a) 275 °C (b) 690 °C and 747 °C temperatures in 100 mHz-32 MHz frequency range.

Using the relationship, $C = (2\pi fR)^{-1}$ where f and R are considered the frequency and resistance of the solid electrolyte circuit; the capacitance of the Nyquist plots at different temperatures using frequency at the maximum point of both semicircles in Figure 5(a) and Figure 5(b) is illustrated on Table 1.

Table 1. Capacitance values and their possible interpretation.

Solid electrolyte	Frequency (Hz)	Resistance (Ω)	Capacitance (F)	Phenomenon responsible (Irvine *et al.,* 1990)
$MgHf_4P_6O_{24}$ (273 °C)	$6.38x10^3$	$3.85x10^5$	$0.65x10^{-12}$	Bulk
45° electrode spike	$2.54x10^2$	$3.17x10^5$	$197.6x10^{-7}$	Sample-electrode interface
$MgHf_4P_6O_{24}$ (690 °C)	$40.3x10^3$	$9.18x10^2$	$4300x10^{-12}$	Bulk
45° electrode spike	$0.101x10^1$	$2.54x10^3$	$6.2x10^{-5}$	Sample-electrode interface
$MgHf_4P_6O_{24}$ (747 °C)	$2.02x10^5$	$3.03x10^2$	$2600x10^{-12}$	Bulk
45° electrode spike	$2.02x10^{-1}$	$11.47x10^2$	$0.7x10^{-5}$	Sample-electrode interface

3.3.1. Temperature Dependence of Ionic Conductivity

In Figure 6, the ionic conductivity of $MgHf_4P_6O_{24}$ solid electrolyte as a function of temperature and activation energy, E_a deduced from the slope of $\ln\sigma_{dc}T\text{-}1000T^{-1}$ plots are $4.52x10^{-4}$ Scm^{-1} and 0.74±0.02 eV at 747 °C, respectively. In this study, the activation energy, E_a signifies enhanced mobility of Mg^{2+}-ions at 747 °C comparable with that earlier published (Adamu *et al.,* 2020).

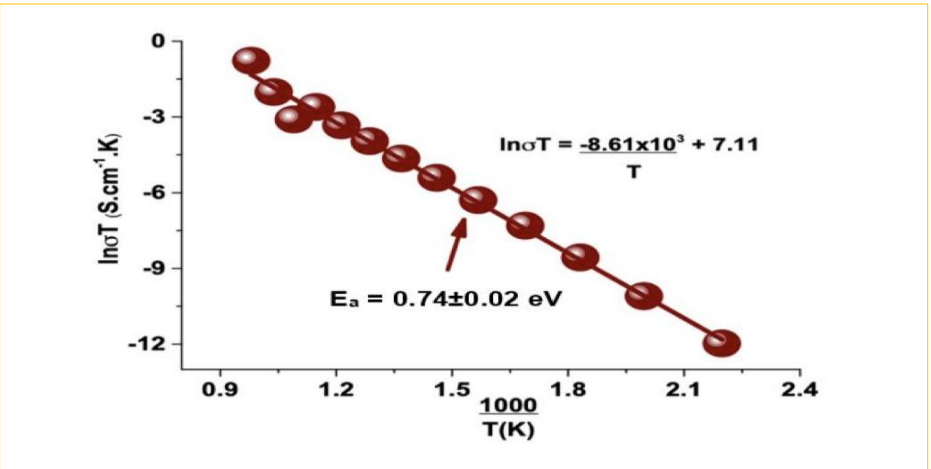

Figure 6. Ionic conductivity of $MgHf_4P_6O_{24}$ solid electrolyte as a function of temperature.

4. Conclusion

Pure homogeneous single phase $MgHf_4P_6O_{24}$ solid electrolyte was successfully prepared using the sol-gel process at a noticeably low temperature. The thermal analysis, TGA-DSC indicated that the solid electrolyte was formed at 900 °C and remained stable at 1300 °C. The ionic conductivity, $\sigma = 4.52 \times 10^{-4}$ Scm^{-1} and activation energy, E_a = 0.74±0.02 eV were achieved at 747 °C. The electrical and electrochemical properties of this solid electrolyte finds potential application in Mg-sensors and other electrochemical devices.

Declarations

Acknowledgments: The authors would like to acknowledge the School of Chemical and Process Engineering, University of Leeds, United Kingdom for the world class facilities provided for this study. Profound appreciation also goes to the Tertiary Education Trust Fund (TETFund) and Kogi State Polytechnic, Lokoja, Nigeria for funding this novel research interest.

Author Contributions: MAA: Study conception and design, data collection, analysis and interpretation of results, manuscript preparation and submission of article; GMK: Manuscript revision and editing.

Conflict of Interest: The authors declare no conflict of interest.

Consent to Publish: The authors agree to publish the paper in International Journal of Recent Innovations in Academic Research.

Data Availability Statement: All relevant data are included in the manuscript.

Funding: This research was funded by the Tertiary Education Trust Fund (TETFund) and Kogi State Polytechnic, Lokoja, Nigeria in the form of Academic Staff Training and Development (PhD Student Grant 2013-2016).

Institutional Review Board Statement: Not applicable.

Informed Consent Statement: Not applicable.
Research Content: The research content of the manuscript is original and has not been published elsewhere.

References

1. Adamu, M. and Kale, G.M. 2016. Novel sol-gel synthesis of $MgZr_4P_6O_{24}$ composite solid electrolyte and newer insight into the Mg^{2+}-ion conducting properties using impedance spectroscopy. Journal of Physical Chemistry C, 120: 17909-17915.
2. Adamu, M., Jacob, K.T. and Kale, G.M. 2020. Assessment of $MgZr_4P_6O_{24}$ as a solid electrolyte for sensing Mg in molten non-ferrous alloys. Journal of the Electrochemical Society, 167(2): 027532.
3. Adamu, M.A. and Kale, G.M. 2025. Structural and thermal stability of sol-gel prepared $MgHf_4P_6O_{24}$ solid electrolyte in molten pre aluminium. Internal Journal of Recent Innovations in Academic Research, 9(3): 294-300.
4. Bauerle, J. 1969. Study of solid electrolyte polarisation by a complex admittance method. Journal of Physics and Chemistry of Solids, 30(12): 2657-2670.
5. Bo, Q.B., Sun, G.X. and Meng, J. 2006. Preparation, structure and oxide ion conductivity in $Ce_{6-x}Y_xMoO_{15-\delta}$(x=0.1-1.4) solid solutions. Journal of Physics and Chemistry of Solids, 67(4): 732-737.
6. Brinker, C.J. and Scherer, G.W. 2013. Sol-gel science: The physics and chemistry of sol-gel processing. Academic Press, New York, 912p.
7. Brinker, C.J., Frye, G.C., Hurd, A.J. and Ashley, C.S. 1991. Fundamentals of sol-gel dip coating. Thin Solid Films, 201(1): 97-108.
8. Chowdari, B.V.R. and Gopalakrishnan, R. 1986. Impedance and modulus spectroscopy of vitreous AgI-Ag_2O-P_2O_5 system. Solid State Ionics, 18: 483-487.
9. Collin, G. and Boilot, J.P. 1989. Superionic solids and solid electrolytes. Academic Press, San Diego.
10. Dislich, H. 1971. New routes to multicomponent oxide glasses. Angewandte Chemie International Edition in English, 10(6): 363-370.
11. Fergus, J.W. 2012. Ion transport in sodium ion conducting solid electrolytes. Solid State Ionics, 227: 102-112.
12. Ferloni, P. and Magistris, A. 1994. New materials for solid state electrochemistry. Le Journal de Physique IV, 4(C1): C1-3- C1-15.
13. Hu, L., Yoko, T., Kozuka, H. and Sakka, S. 1992. Effects of solvent on properties of sol-gel-derived TiO_2 coating films. Thin Solid Films, 219(1-2): 18-23.
14. Huggins, R.A. 2002. Simple method to determine electronic and ionic components of the conductivity in mixed conductors a review. Ionics, 8(3-4): 300-313.
15. Irvine, J.T., Sinclair, D.C. and West, A.R. 1990. Electroceramics: Characterisation by impedance spectroscopy. Advanced Materials, 2(3): 132-138.
16. Joost, W.J. and Krajewski, P.E. 2017. Towards magnesium alloys for high-volume automotive applications. Scripta Materialia, 128: 107-112.
17. Judez, X., Zhang, H., Li, C., Eshetu, G.G., Gonzalez-Marcos, J.A., Armand, M. and Rodriguez-Martinez, L.M. 2018. Solid electrolytes for safe and high energy density lithium-sulfur batteries: Promises and challenges. Journal of the Electrochemical Society, 165(1): A6008-A6016.
18. Knauth, P. 2009. Inorganic solid Li ion conductors: An overview. Solid State Ionics, 180(14-16): 911-916.
19. Livage, J., Henry, M. and Sanchez, C. 1988. Sol-gel chemistry of transition metal oxides. Progress in Solid State Chemistry, 18(4): 259-341.
20. MacDonald, J.R. 1987. Impedance spectroscopy-emphasising solid materials and synthesis, In: Macdonald, J.R., (Ed.), Theory, John Wiley and Sons Inc., New York, 13.
21. Mackenzie, J.D. 1985. Unusual non-crystalline solids from gels in 2004. Journal of Non-Crystalline Solids, 73(1-3): 631-637.

22. Mudenda, S. and Kale, G.M. 2017. Electrochemical determination of activity of Na_2O in $Na_2Ti_6O_{13}$-TiO_2 two phase system between 803-1000 K. Electrochimica Acta, 258: 1059-1063.

23. Mustaffa, N.A. and Mohamed, N.S. 2016. Zirconium-substituted $LiSn_2P_3O_{12}$ solid electrolyte prepared via sol-gel method. Journal of Sol-Gel Science and Technology, 77(3): 585-593.

24. Pathak, A. and Pramanik, P. 2001. Nano-particles of oxides through chemical methods. Proceedings-Indian National Science Academy Part A, 67(1): 47-70.

25. Segal, D. 1997. Chemical synthesis of ceramic materials. Journal of Materials Chemistry, 7(8): 1297-1305.

26. Segal, D.L. 1996. In: Materials science and technology: A comprehensive treatment. Processing of Ceramics, Vol. 17A, (Ed.), Brook, R.J., VCH Publishers, Weinheim, 69p.

27. Sivasankaran, U. and Kumar, K.G. 2019. Electrochemical sensing of synthetic antioxidant propyl gallate: A cost effective strategy using nanoparticles. Journal of the Electrochemical Society, 166(2): B92.

28. Tamura, S., Mori, A. and Imanaka, N. 2004. Li^+ ion conduction in $(Gd, La)_2O_3$-$LiNO_3$ system. Solid State Ionics, 175(1-4): 467-470.

29. Tamura, S., Yamane, M., Hoshino, Y. and Imanaka, N. 2016. Highly conducting divalent Mg^{2+} cation solid electrolyte with well-ordered three-dimensional network structure. Journal of Solid State Chemistry, 235: 7-11.

30. Zelinski, B. and Uhlmann, D.R.J. 1984. Gel technology in ceramics. Journal of Physics and Chemistry of Solids, 45(10): 1069-1090.

Citation: Mohammed Alhaji Adamu and Girish M Kale. 2025. Electrical and Electrochemical Characterisation of Sol-Gel Prepared Magnesium Hafnium Phosphate Solid Electrolyte for Magnesium-Sensors. International Journal of Recent Innovations in Academic Research, 9(3): 337-344.